CHEMISTRY OF MATERIALS

ARTICLE

pubs.acs.org/cm

Sol−Gel Derived Hybrid Thin Films: The Chemistry behind Processing

Alban A. Letailleur,*[,†,‡] François Ribot,[†] Cédric Boissière,[†] Jérémie Teisseire,[‡] Etienne Barthel,[‡] Bernard Desmazières,[§] Nicolas Chemin,[∥] and Clément Sanchez*[,†]

[†]UPMC − Collège de France − CNRS, Chimie de la Matière Condensée de Paris (UMR 7574), 11 place Marcelin Berthelot, 75231 Paris, France

[‡]CNRS − Saint-Gobain, Surface du Verre et Interfaces (UMR 125), 39 quai Lucien Lefranc, 93303 Aubervilliers Cedex, France

[§]Université d'Evry Val d'Essonne − CNRS, Laboratoire Analyse et Modélisation pour la Biologie et l'Environnement (UMR 8587), Boulevard François Mitterrand, 91025 Evry Cedex, France

[∥]Saint-Gobain Recherche, 39 quai Lucien Lefranc, BP 135, 93303 Aubervilliers, France

ABSTRACT: Despite their apparent simple preparation by sol−gel process, silsesquioxanes based materials are quite complex and rich systems. Accordingly, a clear understanding of their elaboration chemistry and its relations to process and properties are important matter. In the particular case of thin film preparation, vitrification must be controlled to ensure high throughput and reliability. Using methylsilsesquioxane based films as a relevant model and a combination of IR spectroscopy, mass spectrometry, and solution ^{29}Si NMR, a meaningful description of the film structure was obtained. Furthermore, vitrification, observed by dynamic mechanical analysis, was shown to depend strongly on the amounts of cages and extended structures present in the films. More interestingly, the proportion of these species can be tuned through a careful control of the elaboration chemistry. On one hand, long aging and high dilution yield a larger amount of cages, which results in a delay of the vitrification. On the other hand, pH appears as the convenient parameter to finely adjust the time span during which high quality films can be prepared from the sols, while preserving the film composition and final properties.

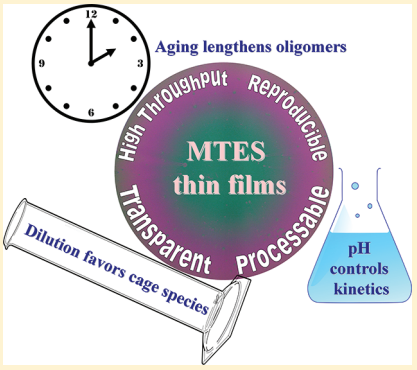

KEYWORDS: silsesquioxane, structure, vitrification, spectroscopy, scaling law

INTRODUCTION

Silsesquioxane based hybrid materials, in particular processed as thin films, have been developed for a large variety of applications. In electronics, they are found in organic electronic devices,[1] for charge trapping,[2] or in low-k coatings.[3] In optics, they are used for luminescence,[4] photochromism,[5] nonlinear optics,[6] or antireflectivity.[7,8] Although complex precursors can be used,[9] such materials can be simply obtained from sol−gel processed organosilicon alkoxides. A key feature in their large development at the industrial scale is the possibility to process them from solutions into different shapes: complex,[10] molecular species,[11] metal clusters,[12] particles,[13] gels or thin films.[14] Furthermore, any organic moiety or codiluted compound can be selected to generate multifunctional materials.[15] Accordingly, a tremendous amount of work has been done on the synthesis of porous films with high surface area[16] or on surface patterning.[17]

One key point in the processing of sol−gel thin films is the control over the vitrification, which corresponds to the appearance of a vitreous state caused by a thermally induced chemical reaction. It defines when a coating is sufficiently cured to allow further processing steps. Actually, the concept of vitrification is not limited to sol−gel chemistry and can be found in the more general framework of reactive materials.[18] Generally speaking, a good knowledge of vitrification is important as it can be used to derive thermorheological behaviors using theories developed for thermosets. In a previous study, we have reported that the vitrification of methylsilsesquioxane derived hybrid materials can be analyzed similarly to thermosetting polymers.[19] Indeed, isothermal studies have shown that the vitrification time follows an exponential decrease with the temperature and is closely related to the internal structure of the film.

Among all the organically modified silanes used to obtain hybrid thin film, methyltriethoxysilane (MTES) appears as the simplest one. Yet, it already yields complex materials, for which the flexibility, which originates from its unreactive organic moiety, enables the processing of thin films,[20] or aerogels.[21] Ro et al. used it, in conjunction with poly(methyl methacrylate), to produce low-k coatings. Using specific synthetic conditions, they prepared highly branched polymethylsislesquioxanes on which polymerization initiators were grafted thanks to the large number of unreacted silanols.[22] Basu and co-workers developed textured thin films for superhydrophobicity and evidenced that the wetting properties and the microstructure were highly dependent on the deposition process.[23]

Moreover, elaboration chemistry and processing appear both to be able to greatly influence the physical properties of silsesquioxanes as illustrated by the following examples. Lebeau et al. showed that the second order nonlinearity of hybrid thin

Received: September 14, 2011
Revised: September 27, 2011
Published: October 18, 2011

films strongly depends on aging and thermal treatment.[24] Masai et al. showed for soft glasses prepared from alkyltriethoxysilanes that the glass transition temperature is reduced when the connectivity is lower or the alkyl side group larger.[25] In their study of MTES derived films, Orel and co-workers demonstrated, using IR spectroscopy, the formation with time of cage species in the sols. According to the influence of these cages on the polarity of the final xerogel, they were able to obtain either hydrophilic or hydrophobic surfaces, by simply modifying the sol aging.[26] More recently, Ro et al., who used mass spectrometry to evidence cage species, explained an increase in the thermal expansion of their MTES derived films by an increase of such cage species during the aging of the sols.[27] However, despite numerous works, a comprehensive study of the effect of the chemistry occurring during processing on the mechanical properties of silsesquioxanes films is still missing.

The present article reports on the influence of the chemistry on the structure and thermorheological behavior of MTES derived films. IR spectroscopy, which is an easy and rapid tool for thin film characterization but often fails to give a clear and complete picture, has been efficiently complemented by mass spectrometry (MS) and ^{29}Si NMR to yield quantitative data on film chemical composition and inner structure. Our results clearly illustrate the large variety of information that can be obtained by such combined techniques on molecular weights, reaction advancement, chemical environments, and bond formation. Moreover, despite the large wealth of species formed by sol−gel process, as reflected by the numerous MS signals and the complex NMR signature, a variation of the elaboration parameters, such as aging, pH, and dilution, leads to a meaningful picture of the chemical reactions and relevant species involved which is further translated in term of materials processing.

EXPERIMENTAL SECTION

Sols were obtained by mixing MTES (2.2 g, 12.5 mmol) with 0.66, 1.42, 3.2, or 6.4 g of a HCl solution to achieve $w = H_2O/Si$ molar ratios of 3, 7, 14, or 28. The pH of the HCl solution was 2.0 to allow for a fast hydrolysis of the precursor and a rather slow condensation. For $w = 14$, the pH of the HCl solution was also varied from 1.0 to 3.0. The originally two-phase systems were vigorously stirred for several minutes, until clear one-phase solutions were obtained, as a result of the release of ethanol and the hydrophilic character of hydrolyzed MTES.

Aging time of the sol (t_a) was measured from the mixing of the reagents. Thin films were prepared by spin-coating the sols (speed: 2000 rpm, acceleration: 500 rpm.s^{-1}, duration: 60 s) on silicon wafers. For an aging time of 5 h, the film thickness is 650 nm ± 20 nm, as measured by both ellipsometry and SEM.

DMA (Dynamic Mechanical Analysis) experiments were performed with a RSA3 apparatus (Rheoservice GmbH, Reichelsheim) on glass fiber mats (50 × 12.5 mm^2 and 0.33 mm thick) that were impregnated with 300 μL of sols and dried under reduced pressure for one hour. Elastic and viscous moduli were measured in tension with a 0.05% elongation strain and a 1 Hz frequency. Evolutions in mechanical properties were measured from 25 to 150 °C with a 4 °C.min^{-1} heating rate. The viscous and elastic moduli of the raw and uncoated glass fiber mats were 1 and 50 MPa, respectively, and did not exhibit any temperature dependence in the explored temperature range.

Infrared spectra of the thin films were collected on a Thermo Nicolet Nexus FTIR spectrometer. Each spectrum was recorded in transmission mode between 650 and 4000 cm^{-1}. The final spectrum was obtained from the average of 32 spectra. Undoped double side polished silicon wafers were used as substrates. All spectra were corrected for the baseline

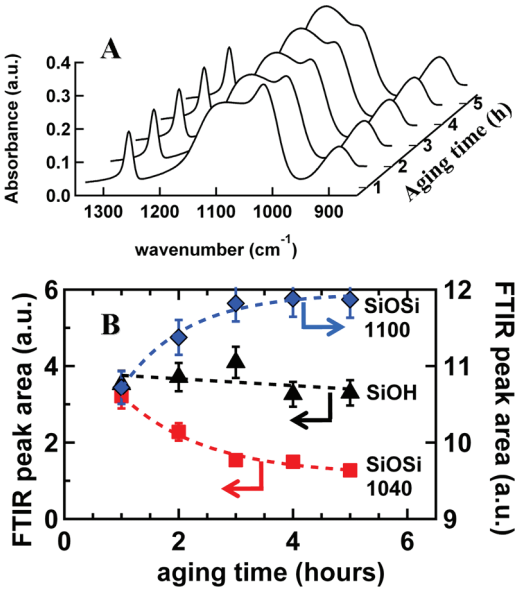

Figure 1. A: FTIR spectra of MTES derived thin films prepared at various aging times. B: Evolution of the FTIR peak area for SiOH (ν = 900 cm^{-1}, left scale), extended Si−O−Si (ν = 1040 cm^{-1}, left scale), and cage Si−O−Si (ν = 1100 cm^{-1}, right scale) signals for thin films obtained from MTES sols after various aging times (dotted lines are guides for the eyes and arrows indicate corresponding axis).

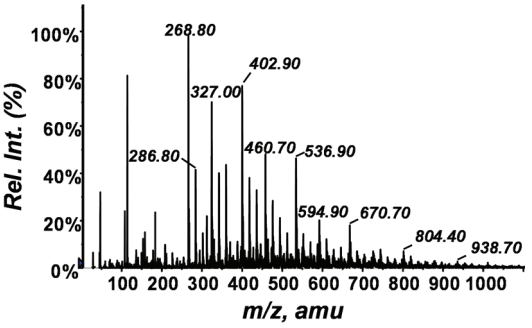

Figure 2. ESI-MS analysis of a methylsilsesquioxane sol aged 2 h 25 min (water/acetonitrile, positive ions).

and normalized with respect to the Si-CH$_3$ peak at 1270 cm^{-1}, which does not show any evolution in the explored temperature range.[28]

Electrospray ionization MS (ESI-MS) spectra were recorded on an API 2000 mass spectrometer (Applied Biosystems) with a turbo ion spray ionization source in the following conditions: liquid samples (5 μL) were introduced into a liquid phase (water/acetonitrile 1:1) flowing at 30 μL·min^{-1}. The source temperature was 100 °C. The capillary voltage was set to +5000 V (respectively −4500 V) for cation (respectively anion) detection. Mass spectra were noise subtracted.

^{29}Si solution NMR was performed on a Bruker 500 Avance^{III} spectrometer (500.13 MHz for ^{1}H and 99.36 MHz for ^{29}Si) equipped with a 10 mm BBO probe. The sols were studied as prepared in 10 mm tubes with a central 3 mm D_2O capillary added for the lock. The ^{29}Si NMR signal was enhanced by DEPT,[29] using a delay of 40 ms and a third ^{1}H pulse of 25°. A recycling delay of 10 s (acquisition time = 1.1 s) was checked to be enough and under such conditions, spectra with a good signal-to-noise ratio were obtained in 12 min, allowing to properly monitor the species along the aging time. As only fully hydrolyzed species are evidenced (vide infra), all silicon atoms are only coupled to a

dx.doi.org/10.1021/cm202755g |Chem. Mater. 2011, 23, 5082–5089

Table 1. Attribution of the MS Peaks Observed in Figure 2 as a Function of the Number of Silicon Atoms and the Number of Condensation Steps in the Species[b]

n (*Si*)	M_n-H^+	- H_2O	- 2 H_2O	- 3 H_2O	- 4 H_2O	- 5 H_2O	- 6 H_2O	- 7 H_2O
2	171	153						
3	247	229	211	193				
4		305	287[a]	269[a] (T^4)				
5			363[a]	345[a]	327[a]			
6			439[a]	421[a]	403[a] (T^6)			
7			515	497[a]	479[a]	461[a]		
8			591	573	555[a]	537[a] (T^8)		
9				649	631	613[a]	595[a]	
10				725	707	689	671[a] (T^{10})	
11				801	783	765	747	729
12				877	859	841	823	805 (T^{12})

[a] Indicates a peak with a relative intensity above 15%. [b] M_n corresponds to $(MeSi)_nO_{n-1}(OH)_{n+2}$, which is the less condensed oligomer for each n value.

single methyl group. Therefore, the obtained ^{29}Si NMR DEPT spectra are quantitative, and the peak areas are proportional to the species concentrations.

RESULTS AND DISCUSSION

Investigation of the Film Structure. IR (Infrared) spectroscopy is a very convenient method to follow in situ the modifications of the film chemical composition during the thermal treatment. Figure 1A displays the FTIR spectra of various fresh MTES derived thin films prepared after different aging times of the sol (w = 14 and pH = 2). Each spectrum shows three contributions in the range 1200-850 cm^{-1}. The present analysis focuses on this peculiar region because it is easily accessible for thin film on a large variety of substrates. The 900 cm^{-1} peak is associated with the SiOH bond, while the signal between 1000 and 1150 cm^{-1} can be assigned to Si−O−Si bonds. A more detailed attribution of the two peaks at 1100 and 1040 cm^{-1} is less straightforward. They cannot be attributed to longitudinal and transverse optical modes, because acquisition under oblique incidence leads to a third peak. The experimental spectrum of the octamethyl-POSS shows a unique contribution at 1115 cm^{-1}.[30] Such a vibration is also observed for a large variety of POSS with a wavenumber between 1100 and 1115 cm^{-1}.[31] Actually, normal-coordinate analyses performed on the octahydro-, octadeutero-, and decahydro POSS (Polyhedral Oligomeric Silsesquioxane) have shown that the IR peak around 1140 cm^{-1}, observed for these cage species, is due to an antisymmetrical stretching mode of the Si−O−Si that is, moreover, exacerbated in cycles containing 4 silicon atoms.[32] The other contribution at 1040 cm^{-1} is due to the symmetrical stretching mode of Si−O−Si bonds that is stronger in more extended and less constrained structures.[33] Figure 1B shows the evolution of the areas of the IR bands at 900, 1040, and 1100 cm^{-1} for thin films prepared after various aging times of the sols. The amount of SiOH bonds shows very little variations with t_a, which means that the number of Si−O−Si bonds is almost constant in all the films. However, the structure of the Si−O−Si skeleton appears strongly affected by aging. Indeed, the ratio cage/extended structures increases when the sol is aged.

Mass spectrometry analysis of the sols was carried out, using classical electro spray ionization. Figure 2 gives the mass spectrum of a MTES sol aged 2 h 25 min (pH 2 and w = 14). All the peaks data can be interpreted taking into account only hydrogen adducts. The results are gathered in Table 1 in which the masses are displayed according to the number of silicon atoms (from 2 to 12) and intramolecular condensation steps. The main peaks (relative intensity higher than 15%) have been labelled. The column labeled M_n-H^+ corresponds to the first oligomers of each series, $(MeSi)_nO_{n-1}(OH)_{n+2}H^+$, which result from n-1 condensations between n methylsilanetriol units. The following columns correspond to the oligomers that have undergone additional intramolecular condensation steps. In the sol, only a little amount of purely linear objects is observed, and the majority of species corresponds to oligomers that have gone through several internal condensation steps, including the fully condensed ones that are cage species. These objects have been described in the literature and are known as T^4, T^6, T^8, T^{10}, ... here the superscript refers to the number of silicon atoms,[34] and have been widely used in the mechanical and thermal reinforcement.[35] They are fairly inert and act as dead-ends in the reaction chains. MS analysis performed at various aging times shows that the amount of cage-species and the average mass of the nonfully condensed species both increase during the aging of the sols.

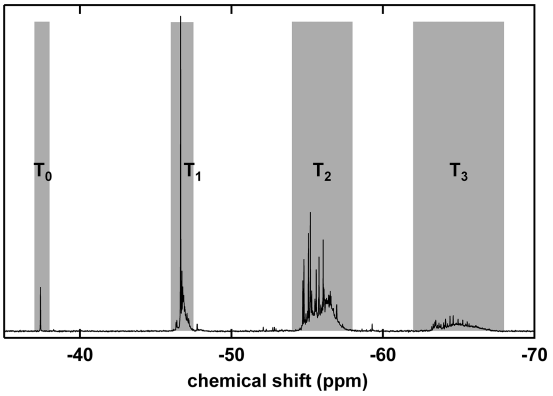

Figure 3. ^{29}Si NMR spectra of MTES sols aged 3 h 45 min at pH 2. The gray areas indicate the T_i regions used for the integration.

The sols, from which the films were prepared, were also investigated by ^{29}Si NMR at various aging times. Figure 3 shows the NMR spectrum for a sol (w = 14 and pH = 2) aged 3 h 45 min.

dx.doi.org/10.1021/cm202755g |*Chem. Mater.* 2011, 23, 5082–5089

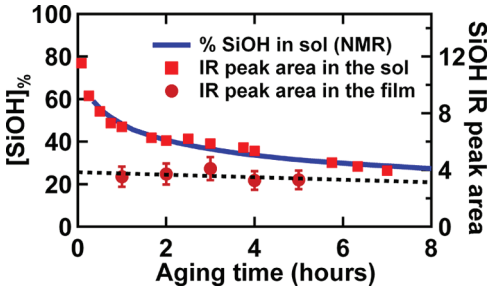

Figure 4. Evolution of the SiOH bonds amount with the aging time of the sol. Concentration of SiOH bonds inside the MTES sol calculated from NMR data (solid line and left scale). SiOH FTIR peak area (right scale) for the sol (squares) and thin films (circles).

The gray areas in Figure 3 indicate the T_i regions from which the integrals were computed.[36] Right from the first spectrum (t_a = 12 min, i.e. when a single phase is obtained), a unique T_0 (uncondensed) species is observed, which indicates that MTES is rapidly fully hydrolyzed to yield $CH_3Si(OH)_3$. A few minor signals appear outside the defined T_i regions. They actually account for a very minute amount of species. They are related to very constrained cycles with three silicon atoms, whereas the signals associated with four-member rings are not downfield shifted and appear, therefore, in the regular T_i regions.[29,31]

^{29}Si NMR allows computing the percentage of remaining SiOH ($[SiOH]_{\%}$) from the relative amounts of T_i species ($[Ti]_{\%}$)

$$[SiOH]_{\%} = \sum_{i=0}^{3} \frac{(3-i)}{3}[T_i]_{\%} \quad (1)$$

Figure 4 reports the evolution of $[SiOH]_{\%}$ in the sol as a function of the aging time. After t_a = 1 h, $[SiOH]_{\%}$ equals 48% and reaches 32% after 5 h. The aging of the sol was also studied with IR spectroscopy and the evolution of the SiOH peak area compared with NMR results. The same evolution is observed in both experiments. Accordingly, the right scale of Figure 4 was adjusted so that the IR peak area matches the $[SiOH]_{\%}$ on the left scale. This comparison between the NMR and IR data in the sol leads to a quantitative analysis of the IR results that can be further used for the films. Therefore, Figure 4 displays also the area of the IR peak (900 cm^{-1}) associated with SiOH bonds for thin films deposited after various t_a. The percentage of SiOH remaining in the film right after the deposition is around 25% and shows almost no variation with aging time. Accordingly, some condensation of the silica network occurs during the deposition, especially for short aging times.

At short t_a, small oligomers are present in the sol, and more condensation is required to obtain the same SiOH relative amount in a continuous film. Due to the reduced mobility and short time involved, the condensation that takes place during deposition leads preferentially to extended forms. For longer t_a, more cage species are present in the sol, as evidenced by MS, and are deposited without modifications in the films. In addition to IR and MS data, the formation of cage species in the sol during aging is indeed supported by the appearance of a precipitate, instead of a gel, at long aging.

Influence of the Chemistry on Dynamic Thermomechanical Behavior. These modifications in the chemical structure of the film induce different mechanical properties. Using Dynamic Mechanical Analysis, the evolution of tan δ, the ratio of the viscous to elastic modulus, was recorded during temperature ramps for various t_a. The vitrification temperature, which can be

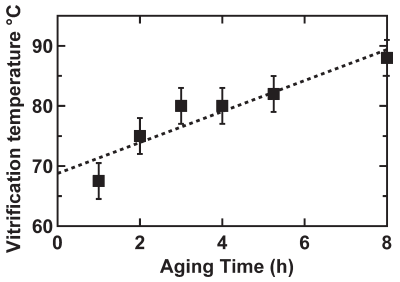

Figure 5. Evolution of the vitrification temperatures (T_v) for various aging times. The vitrification temperature was measured from the second maxima of tan δ vs T curves in DMA experiments.

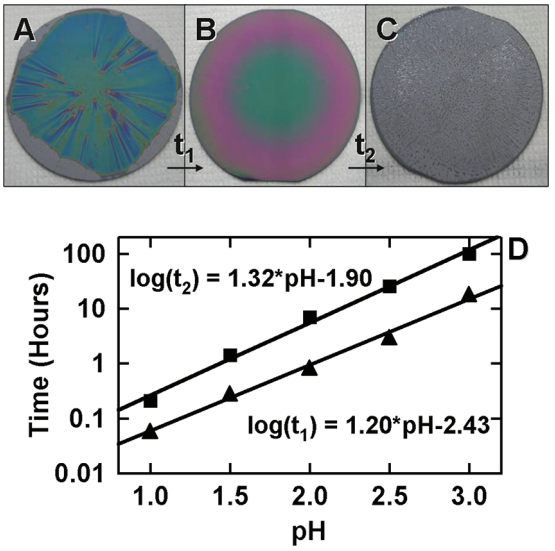

Figure 6. Pictures of thin films prepared after a too short (A, before t_1), an optimal (B, between t_1 and t_2), and a too long (C, after t_2) aging time. Evolution with pH of the times t_1 (triangles) and t_2 (squares), between which a homogeneous coating is obtained (D). Solid lines and equations result from the best linear fit of the data.

associated with the second maximum in the curve tan δ vs T,[19] is displayed in Figure 5 for various aging times. It is significantly affected by the aging of the sol, increasing with t_a. Such an evolution with t_a is far from minor as a previous study has shown that a difference of only 10 °C in the vitrification temperature results in a two to three times longer vitrification process.[19] For long t_a, there are initially less extended Si−O−Si bonds (Figure 1B). Therefore more reactions are needed to obtain a vitrified material. In terms of material processing, this leads to longer curing time for longer aging and reduces the process throughput. Moreover, this control over the fine structure of the film enables adjusting the residual stress inside the layer.[37] More cage species lower the effective cross-linking in the film and make the stress relaxation easier.

Scaling the Kinetics with pH. Difference in aging of a couple of hours induces strong modification of the thermomechanical properties of the films. A control over the kinetics is therefore required to make the process more flexible. Along with suitable mechanical properties, the optical quality of the coating can also be important for the foreseen application. For the methylsilsesquioxane derived thin film studied, homogeneous and transparent coatings can only be obtained from the sol in a limited range

dx.doi.org/10.1021/cm202755g |*Chem. Mater.* 2011, 23, 5082–5089

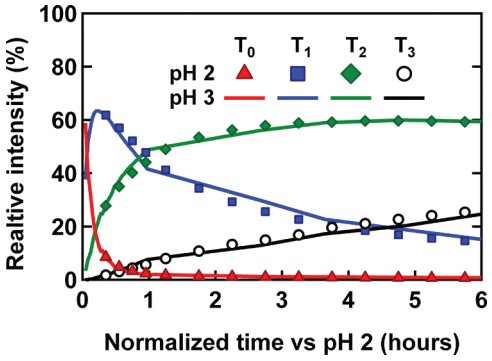

Figure 7. Intensities of the T_i (i = 0..3) species observed in ^{29}Si NMR during the aging of a sol prepared with pH 2 (marks) and pH 3 (lines). The time scale of the pH 3 experiment was divided by 20 for normalization.

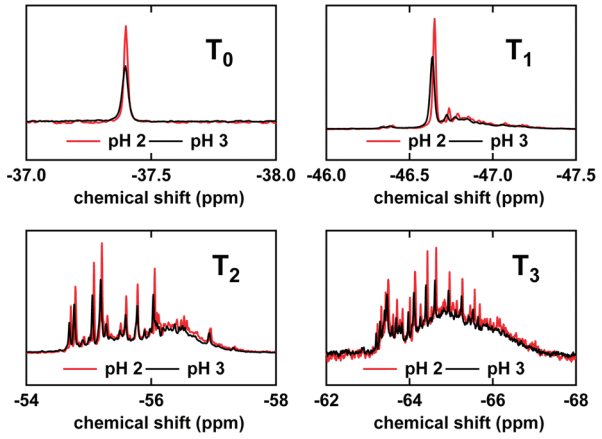

Figure 8. Zooms of the T_i regions for ^{29}Si NMR spectra of MTES sols aged 3 h 45 min at pH 2 (red) or 73 h at pH 3 (black).

of aging time. For short t_a, the oligomers in the sol are too short and cannot create a continuous film (Figure 6A). For long aging, the cage species start to precipitate, due to their hydrophobic character, and the film scatters light (Figure 6C). The transitions are sufficiently sharp to define accordingly two times t_1 and t_2, both measured from the mixing of the reagents, between which optically transparent films are obtained (Figure 6B). More precisely, t_1 is the minimum aging required to obtain full coverage of the substrate by the coating, whereas t_2 corresponds to the minimum aging that leads to a scattering film. For instance, at pH 2, t_1 is around an hour and t_2 equals six hours. Figure 6D reports these t_1 and t_2 times for pH ranging from 1 to 3. At pH 1, homogeneous films can be obtained only during a few minutes after the start of hydrolysis, whereas the solution is stable for several days at pH 3. This very large difference in t_1 and t_2 can be explained by the difference in kinetics. The condensation reaction is activated by charged species, and its kinetics reaches a minimum at the isoelectric point of the growing siloxane based oligomers. For hydrolyzed MTES, isoelectric point is reported around 3.5, a higher value than for silica due to the donor effect of the methyl group.[38] For lower pH, the kinetics is proportional to the concentration of protonated species. The slope of the curve $\log(t_1)$ vs pH should therefore be one. The observed slopes are 1.20 and 1.32 for t_1 and t_2, respectively, which means that the modification of the kinetics via a protonation mechanism is

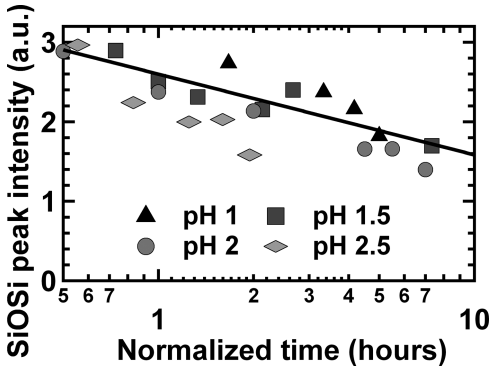

Figure 9. Area of the extended Si−O−Si IR peak (ν = 1040 cm^{-1}) for methylsilsesquioxane thin films prepared from sols at pH 1, 1.5, 2, and 2.5 after various aging time. The time scales were normalized with respect to the pH 2, by the factor t_1(pH x)/t_1(pH 2) (Figure 6). The solid line corresponds to the best linear fit of all the data points.

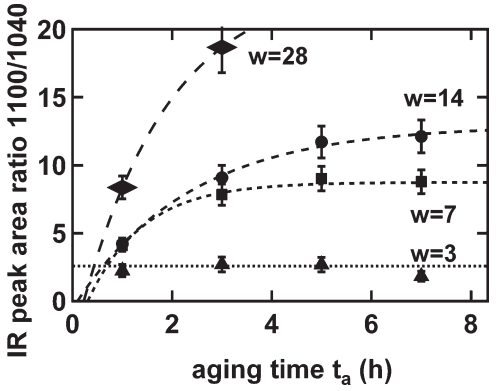

Figure 10. Evolution with aging time of the ratio of the area of the FTIR band related to Si−O−Si cage (ν = 1100 cm^{-1}) to the one related to the extended Si−O−Si (ν = 1040 cm^{-1}) for methylsilsesquioxane thin film prepared from sols at w = 3, 7, 14, and 28.

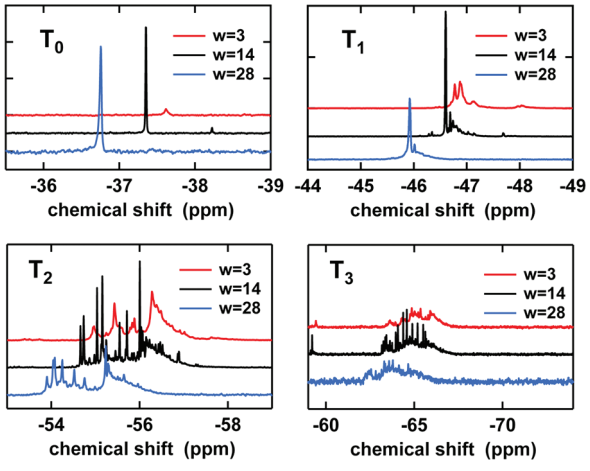

Figure 11. ^{29}Si NMR intensities of the T_i (i = 0..3) species observed during the aging of a sol prepared from pH 2 with w = 3 (red), 14 (black), and 28 (blue).

the main effect of the pH. However, the relationship between kinetics and pH has been only shown for the silanetriol and

dx.doi.org/10.1021/cm202755g |Chem. Mater. 2011, 23, 5082–5089

Scheme 1. Summary of the Influence of the Key Parameters (Aging, pH, Dilution) To Obtain the Targeted MTES Film with Optical Transparency, Right Mechanical Behavior, and High Throughput

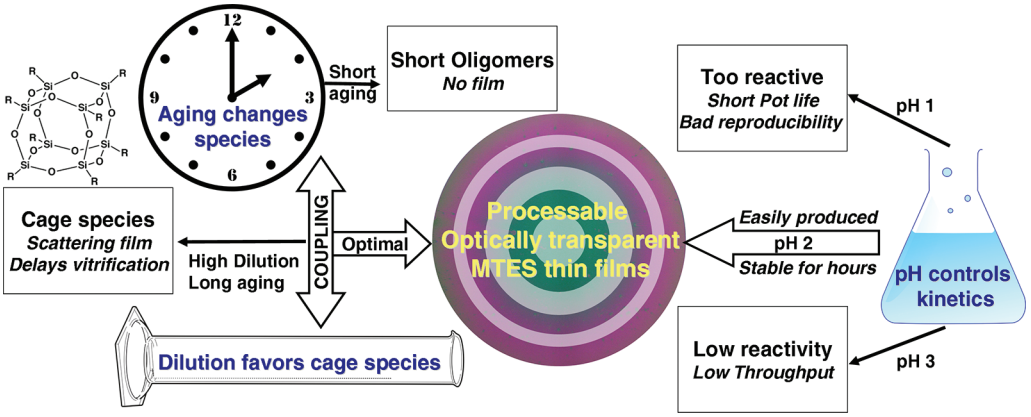

evolves during the condensation. This explains why the obtained slope values are slightly larger than one.

The scaling law observed for the deposition windows with pH does not imply that the species formed during aging are the same. The evolution of the relative T_i concentrations is reported in Figure 7 for the first six hours of aging time, at pH 2.0 (the integrated regions are those pictured in Figure 3). The T_0 signal is relatively weak and, along with the T_1 signal, shows a constant decrease with aging. After a couple of hours, the T_2 peak reaches a steady state at *ca.* 60%. During aging, the T_3 signal keeps on increasing, in agreement with a progressive cross-linking and the formation of cage species.

^{29}Si NMR experiments were also carried out during aging at pH 3. The relative T_i concentrations are reported as solid lines in Figure 7. The curves exhibit a very good match between both pH when the aging time at pH 3 was divided by 20, which is the ratio between t_1 for pH 3 and for pH 2. Accordingly, the scaling law for the condensation kinetics is identical to the one observed for the deposition process. Moreover, the ^{29}Si NMR spectra (Figure 8) obtained at pH 2 after 3 h 45 min aging and at pH 3 after 73 h (ca. 20 times more) are very similar. A small variation in their line width likely arises from slightly different field homogeneity in the samples. This match clearly shows that, when the pH is modified, not only the general evolution but also the created species are the same (yet after a longer aging). As the effect of the pH on the evolution of the deposition windows (Figure 6) and on the evolution of the kinetics (Figure 7) is the same, the optical quality of the films depends mainly of the species present in the sol at the deposition time.

The impact of the deposition process on the structure of the films was also studied. Figure 9 reports the area of the extended Si−O−Si IR peak (1040 cm^{-1}) as a function of a normalized aging time for pH 1, 1.5, 2, and 2.5. For each pH the abscissa was rescaled, as explained above, according to the t_1 evolution presented in Figure 6. The decreasing trend in the intensity of the extended Si−O−Si species is similar at all pH and yield the same scaling law than previously (the best linear fit for all the data points is also presented in Figure 9). Nevertheless, for equivalent normalized aging, the formation of extended Si−O−Si appears more pronounced at low pH for which a higher condensation is also observed, as indicated by a lower SiOH peak area. Actually, even if the evolution in the sol is similar for all pH, condensation does also occur during the deposition process and is therefore more pronounced at low pH where the kinetics is higher.

To conclude on this part, lowering the pH causes an acceleration of the condensation kinetics. More interestingly, the fine chemical composition of the sol during aging is not affected by pH and little variations are observed in the films. For the process point of view, pH appears therefore as an almost completely independent parameter to be considered for tuning the process time and throughput.

Increase of Cage Species in Diluted Media. The creation of the cage species impacts strongly the thermomechanical behavior of the hybrid thin films by increasing the vitrification temperature. Changing the dilution of hybrid molecules in solution may lead to the modification of the formation kinetics of these cage species and offers another way to control the mechanical properties of the films. To check this point, sols were synthesized with various $w = H_2O/Si$ ratios, respectively 3, 7, 14, and 28 at pH 2. For $w = 28$, the sol shows a poor stability in time and precipitates after 4 h of aging. On the contrary, reducing the amount of water leads to greater t_2 time, meaning that films can be obtained from the solution after 9 h of aging. These observations are in line with the variations of pH of the resulting sols which accelerate (high w) or slow down (low w) the condensation kinetics. Another explanation lies in the preferential formation of different species in more diluted medium. Figure 10 presents for the four different w values the ratio of the IR peak intensity at 1100 cm^{-1} (cage) over the one at 1040 cm^{-1} (extended) for thin films prepared at various aging times. As already observed in Figure 1, aging leads to the formation of cage species. Moreover, increasing the dilution of the sol leads to an acceleration of this formation. Indeed, the intramolecular condensation is promoted in diluted media and enables a faster formation of these cage species. However, because in these highly condensed species the hydrophobic methyl moiety points outward, their stability in water rich medium is reduced and explains why precipitation is rapidly observed for $w = 28$.

To further investigate the formation of cage species, ^{29}Si NMR spectra of sol, prepared with w equals 3, 14, and 28, were recorded during sol aging. Figure 11 presents zooms of the four T_i regions for three samples with the same SiOH relative concentration (40%), i.e. with the same condensation. They correspond to aging times of 3 h, 2 h, and 3 h 20 min for w of 3, 14, and 28, respectively. The observed high frequency shift

dx.doi.org/10.1021/cm202755g |*Chem. Mater.* 2011, 23, 5082–5089

when w increases can be explained by a larger fraction of water which modifies the surrounding medium.[29] However, simple translations along the chemical shift axis do not lead to superimpose spectra. For the higher values of w, the contributions on the high frequency side of the T_2 and T_3 massifs are more important. As these regions have been previously assigned to cage cyclic species,[39] ^{29}Si NMR brings another evidence for the preferential formation of cage species during aging in diluted media.

CONCLUSION

This study emphasizes the high complexity of hybrids sol−gel systems in term of species formed during processing. A precise understanding of the link between the elaboration chemistry and the targeted properties is a requirement to achieve high throughput and quality, yet it is often underestimated in the process. MS, ^{29}Si NMR, and IR spectroscopies were jointly used to assess the chemical composition of the MTES derived sols and films and relate it to their thermomechanical properties. Scheme 1 presents how the chemical and processing parameters must be coupled to efficiently achieve the targeted properties: simple and fast fabrication of optically transparent and mechanically processable MTES thin films. The chemistry behind engineering described in this article is paramount to reproducibly obtain nanostructured sol−gel derived hybrid coatings. During aging, the formation of cage species, analog to POSS, has been evidenced. As they do not participate to the network formation their incorporation in the thin film structure induces a delay in the vitrification. Furthermore, as they are mainly hydrophobic, their stability in solution is rather limited and causes light scattering in the film. Increasing the sol dilution promotes also the formation of cage species, yet with only minor alterations of the overall kinetics. Finally, the overall process time and throughput can be independently controlled by the pH. The aging of the sol may be adjusted between a few minutes and a few days (the lower the pH, the faster the condensation), yet without any modifications in the chemical microstructure. Therefore, a fine combination of the elaboration chemistry parameters enables the tuning of the process from the solution to the thin film. Finally, this work establishes a framework for the analysis and the processing of sol−gel derived hybrid silica coating. It can be used for more complex and functional materials with larger and more complex side groups. Even if the side group has a strong impact on the reactivity and solubility of the organosilane, the effect of aging, pH, and dilution described here should be comparable.

AUTHOR INFORMATION

Corresponding Author

*Phone: +33 1 48 39 59 56. Fax: +33 1 48 39 55 62. E-mail: alban.letailleur@saint-gobain.com (A.A.L.), clement.sanchez@upmc.fr (C.S.).

ACKNOWLEDGMENT

Maxime Chestier and Benoit Didier are acknowledged for valuable discussion on DMA. The authors thank Saint-Gobain Research for funding.

REFERENCES

(1) Lim, Y.; Park, Y.-S.; Kang, Y.; Jang, D. Y.; Kim, J. H.; Kim, J.-J.; Sellinger, A.; Yoon, D. Y. *J. Am. Chem. Soc.* **2011**, *133*, 1375–82.
(2) Choi, J.-K.; Jang, S.; Kim, K.-J.; Sohn, H.; Jeong, H.-D. *J. Am. Chem. Soc.* **2011**, *133*, 7764–85.
(3) Rathore, J. S.; Interrante, L. V.; Dubois, G. *Adv. Funct. Mater.* **2008**, *18*, 4022–4028.
(4) Fernandes, M.; Zea Bermudez, V.; de; Sá Ferreira, R. a; Carlos, L. D.; Charas, A.; Morgado, J.; Silva, M. M.; Smith, M. J. *Chem. Mater.* **2007**, *19*, 3892–3901.
(5) Levy, D. *Chem. Mater.* **1997**, *9*, 2666–2670.
(6) Jiang, H.; Kakkar, A. K. *J. Am. Chem. Soc.* **1999**, *121*, 3657–3665.
(7) Du, Y.; Luna, L. E.; Tan, W. S.; Rubner, M. F.; Cohen, R. E. *ACS Nano* **2010**, *4*, 4308–16.
(8) For a review, see:Lebeau, B.; Innocenzi, P. *Chem. Soc. Rev.* **2011**, *40*, 886–906.
(9) Dhayal, V.; Bohra, R.; Nagar, M.; Kaushik, A.; Mathur, S.; Barth, S. *Appl. Organomet. Chem.* **2008**, *22*, 629–636.
(10) Sakamoto, N.; Ikeda, C.; Yamamura, M.; Nabeshima, T. *J. Am. Chem. Soc.* **2011**, *133*, 4726–9.
(11) (a) Asuncion, M. Z.; Laine, R. M. *J. Am. Chem. Soc.* **2010**, *132*, 3723–36. (b) Thompson, D. B.; Brook, M. A *J. Am. Chem. Soc.* **2008**, *130*, 32–3.
(12) Tan, G.; Yang, Y.; Chu, C.; Zhu, H.; Roesky, H. W. *J. Am. Chem. Soc.* **2010**, *132*, 12231–3.
(13) Hu, L.-C.; Khiterer, M.; Huang, S.-J.; Chan, J. C. C.; Davey, J. R.; Shea, K. J. *Chem. Mater.* **2010**, *22*, 5244–5250.
(14) Sanchez, C.; Belleville, P.; Popall, M.; Nicole, L. *Chem. Soc. Rev.* **2011**, *40*, 696–753.
(15) (a) Hu, L.-C.; Shea, K. J. *Chem. Soc. Rev.* **2011**, *40*, 688–95. (b) Olkhovyk, O.; Jaroniec, M. *J. Am. Chem. Soc.* **2005**, *127*, 60–61.
(16) (a) El Kadib, A.; Hesemann, P.; Molvinger, K.; Brandner, J.; Biolley, C.; Gaveau, P.; Moreau, J. J. E.; Brunel, D. *J. Am. Chem. Soc.* **2009**, *131*, 2882–92. (b) Yang, Y.; Sayari, A. *Chem. Mater.* **2008**, *20*, 2980–2984. (c) Sakamoto, S.; Shimojima, A.; Miyasaka, K.; Ruan, J.; Terasaki, O.; Kuroda, K. *J. Am. Chem. Soc.* **2009**, *131*, 9634–5. (d) Sayari, A.; Belmabkhout, Y. *J. Am. Chem. Soc.* **2010**, *132*, 6312–4.
(17) (a) Liu, L.; Toledano, R.; Danieli, T.; Zhang, J.-Q.; Hu, J.-M.; Mandler, D. *Chem. Commun.* **2011**, *47*, 6909–11. (b) Wang, Y.-W.; Chen, W.-C. *Mater. Chem. Phys.* **2011**, *126*, 24–30. (c) Ahmad, S. A A.; Wong, L. S.; Ul-Haq, E.; Hobbs, J. K.; Leggett, G. J.; Micklefield, J. *J. Am. Chem. Soc.* **2011**, *133*, 2749–59.
(18) Enns, J. B.; Gillham, J. K. *J. Appl. Polym.* **1983**, *28*, 2567–2591.
(19) Letailleur, A.; Teisseire, J.; Chemin, N.; Barthel, E.; Sondergard, E. *Chem. Mater.* **2010**, *22*, 3143–3151.
(20) Rao, A. V.; Latthe, S. S.; Mahadik, S. A.; Kappenstein, C. *Appl. Surf. Sci.* **2011**, *257*, 5772–5776.
(21) Aravind, P. R.; Soraru, G. D. *J. Porous Mater.* **2010**, *18*, 159–165.
(22) Ro, H. W.; Kim, K. J.; Theato, P.; Gidley, D. W.; Yoon, D. Y. *Macromolecules* **2005**, *38*, 1031–1034.
(23) Basu, B. J.; Hariprakash, V.; Aruna, S. T.; Lakshmi, R. V.; Manasa, J.; Shruthi, B. S. *J. Sol-Gel Sci. Technol.* **2010**, *56*, 278–286.
(24) Lebeau, B.; Brasselet, S.; Zyss, J.; Sanchez, C. *Chem. Mater.* **1997**, *9*, 1012–1020.
(25) Masai, H.; Takahashi, M.; Tokuda, Y.; Yoko, T. *J. Mater. Res.* **2005**, *20*, 1234–1241.
(26) Orel, B.; Jese, R.; Vilcnik, A.; Lavrencic Stangar, U. *J. Sol-Gel Sci. Technol.* **2005**, *34*, 251–265.
(27) Ro, H. W.; Park, E. S.; Soles, C. L.; Yoon, D. Y. *Chem. Mater.* **2010**, *22*, 1330–1339.
(28) Tejedor-tejedor, M. I.; Paredes, L.; Anderson, M. A. *Chem. Mater.* **1998**, *10*, 3410–3421.
(29) Brunet, F. *J. Non-Cryst. Solids* **1998**, *231*, 58–77.
(30) Handke, B.; Jastrzębski, W.; Mozgawa, W.; Kowalewska, A. *J. Mol. Struct.* **2008**, *887*, 159–164.
(31) Cordes, D. B.; Lickiss, P. D.; Rataboul, F. *Chem. Rev.* **2010**, *110*, 2081–173.
(32) Marcolli, C.; Lainé, P.; Bühler, R.; Calzaferri, G.; Tomkinson, J. *J. Phys. Chem. B* **1997**, *101*, 1171–1179.
(33) Park, E. S.; Ro, H. W.; Nguyen, C. V.; Jaffe, R. L.; Yoon, D. Y. *Chem. Mater.* **2008**, *20*, 1548–1554.

(34) (a) Brown, J. F.; Vogt, L. H.; Prescott, P. I.; Prescott, P. I. *J. Am. Chem. Soc.* **1964**, *86*, 1120–1125. (b) Voronkov, M. G.; Lavrent'yev, V. I. *Top. Curr. Chem.* **1982**, *102*, 199–236.

(35) Tanaka, K.; Adachi, S.; Chujo, Y. *J. Polym. Sci., Polym. Chem.* **2009**, *47*, 5690–5697. (b) Tanaka, K.; Ishiguro, F.; Chujo, Y. *J. Am. Chem. Soc.* **2010**, *132*, 17649–51.

(36) T_i species correspond to silicon atoms condensed with *i* other silicon atoms through SiOSi bonds.

(37) Atanacio, A. J.; Latella, B. A.; Barbé, C. J.; Swain, M. V. *Surf. Coat. Technol.* **2005**, *192*, 354–364.

(38) Brinker, C. J.; Scherer, G. W. *Sol-gel Science: The Physics and Chemistry of Sol-Gel Processing*; Academic Press: San Diego, CA, 1990; Chap. 3.

(39) Lebeau, B.; Maquet, J.; Sanchez, C.; Toussaere, E.; Hierle, R.; Zyss, J. *J. Mater. Chem.* **1994**, *4*, 1855–1860.